

A Hierarchical Matching for Amery Ice Shelf Surface Motion Estimation from Repeat Satellite Imagery

<http://dx.doi.org/10.3991/ijoe.v9iS7.3194>

Yi Liu, Fei Yan and Weian Wang
Tongji University, Shanghai, China

Abstract—In this paper, remote sensing data of Amery ice shelf was used to study Antarctica ice motion and flux problem by a hierarchical image matching method. It combines feature points and grid points to provide a dense, precise and reliable matching result. First, seed points are extracted at the top level of image pyramid using the SIFT algorithm with RANSAC approach to remove mismatches and enhance robustness. These points are used to construct an initial triangulation. Then, feature point and grid point matching are conducted based on the triangle constraint. In the process of hierarchical image matching, the parallaxes from upper levels are transferred to levels beneath with triangle constraint. At last, outliers are detected and removed based on local smooth constraint of parallax. Also, bidirectional image matching method is adopted to verify the matching results and increase the number of matched points. Experiments with Landsat7 images show that the proposed method has the capacity to generate reliable and dense matching results for surface velocity estimation from stereo satellite imagery. Global warming will lead to Amery shelf and glaciers melt and flow rate increase, which can be confirmed by on-site GPS and remote sensing data. Through research the ice shelf flow velocity field, the bottom can calculate the ice flux of this area, and result confirm that the impact of climate for glacier and ice shelf.

Index Terms—Amery ice shelf(AIS), Global warming, Lambert glacier, ice flow.

I. INTRODUCTION

The Amery Ice Shelf (AIS) (figure 1-1) is the third largest embayed shelf in Antarctica. It is main thoroughfare of the East Antarctic ice sheet material flows into Atlantic. In the current context of global warming, Amery Ice Shelf's slight changes will exert huge impact on the world environment and global climate. It drains the grounded ice from the interior of the Lambert Glacier drainage basin, which covers 16% of the mass of the East Antarctic ice sheet and is the world's largest glacier by volume[2]. The Lambert Glacier is up to 65 km wide and 400 km long, and drains about 8% of Antarctica's ice sheet to AIS. Today, however, people lack of awareness on the Antarctic ice shelf dynamic deformation characteristics and stability, especially the mechanisms of the surface and inside motion is far from in-depth understanding.

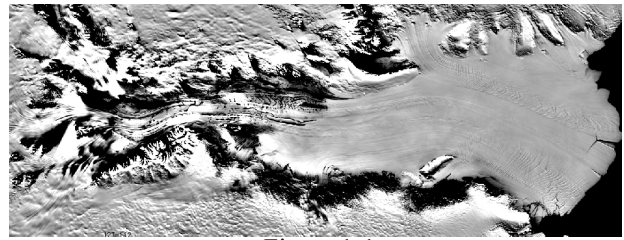


Figure 1-1

Antarctic ice sheet is the past global climate change best record carrier. Antarctic ice sheet with its continuous deposition, the deposition volume per unit time, fewer epigenetic disruption, preservation of the past climate and environmental change resolution, continuous record. This is also the country competed in the Antarctic glacier research carried out mainly. Polar regions to global climate change "Amplifier" role. Historical and modern observations have shown that the magnitude of polar climate change is medium / low latitudes 2 times, indicating that the polar easier to monitor in the middle and low latitudes imperceptible to the subtle changes.

From interferometric analysis of RADARSAT SAR data, Young etc. generated a dense network of surface velocity vectors over the AIS. Ice speeds decrease downstream from about 800 near the confluence of major ice streams at the grounding zone to less than 350 . They then increase to nearly 1400 m a-1 at the centre of the calving front. Young derived the strain rate fields over the AIS from these velocities.

Image matching and feature tracking technique also can be used to measure surface velocity of ice flow. It is to study how to choose some features and similar standards based on the reference image and searching image to search for strategies for correlation computing and to determine the best space responding point for matching. Its main issues focus on the feature space, similarity measurement and searching strategies. The fatal step is to ascertain effective matching methods; a good matching method requires high reliability, small error, fast speed and good real-time.

Image matching is relatively easy when encountered with good image texture conditions. However, on relatively poor textural images, image matching is a difficult and challenging problem. Most of the traditional digital photogrammetry systems require lots of human interactions to remove the errors in the matching results when dealing with poor textural images.

In this paper, a triangulation-based hierarchical image matching algorithm for stereo satellite imagery is described. It uses a coarse-to-fine hierarchical strategy and combines feature points and grid points to provide a dense, precise and reliable matching result. First, some seed points are extracted at the top level of image pyramid using the SIFT algorithm with RANSAC approach to remove mismatches and enhance robustness. These points are used to construct an initial triangulation. Then, feature point and grid point matching are conducted based on the triangle constraint. In the process of hierarchical image matching, the parallaxes from upper levels are transferred to levels beneath with triangle constraint. At last, outliers are detected and removed based on local smooth constraint of parallax. Also, bidirectional image matching method is adopted to verify the matching results and increase the number of matched points. Experiments with Landsat images show that the proposed method has the capacity to generate reliable and dense matching results from stereo satellite imagery.

In the process of projection from three-dimensional world to two-dimensional images, a lot of information is lost and it is an ill-posed problem. So we must make the best of constraints included in the problem to be solved to limit the size of solution space. After the computation of matching, in reality, there are complex situations such as occlusion, shadows, poor texture, atmospheric dust and steep terrain. So there may be some wrong correspondences and constraints are necessary to eliminate blunders. For now, the common constraints for image matching in digital photogrammetry are mainly as follows:

- 1) Similarity constraint. Corresponding points are assumed to have similar intensity or colour. So intensity is the main information used in stereo matching.
- 2) Continuity constraint. Surfaces of objects are assumed to be smooth, which means its parallax varies continuously.
- 3) Uniqueness constraint. Uniqueness constraint is that searching for matching point on the right image, taking left image as reference, matching point with right image and reference point with left image should be consistent.

II. MATCHING METHODS REVIEW

In the last few decades, a lot of efforts have been devoted in the field of photogrammetry and computer vision to improve the reliability, automation, and efficiency of image matching which can be generally divided into two classes based on the matching primitives. One is area-based matching and the other is feature-based matching.

Area-based Matching: Area-based matching usually works directly on local image windows, and it can acquire dense correspondences. It uses the grey value of the whole image to measure the similarity of two images directly. And a certain method is employed to search the point where the similarity measurement is the biggest. There are many area-based matching methods such as Maximization of Mutual Information, correlation method, conditional entropy method, joint entropy method and so on. Although area-based matching is the most widely

used, there exists some shortcomings such as huge computation, long time of matching and sensitivity to rotating, scaling and distort.

Feature-based matching: The common image feature includes point feature, straight line, edge, shape, closed area, statistical moment, etc. By far, feature extraction algorithm can be divided into three main classes: one is point feature extraction operator such as Förstner operator, Harris operator and SUSAN operator, the second is linear feature extraction operator (such as Canny operator, LoG operator), and the third is surface extraction operator mainly through region segmentation. Generally speaking, feature-based matching has the advantage of being simple to operate, rapid matching speed and high precise matching rate, but it also requires human intervention and the obtaining of feature points is a bit difficult. Besides, it is only suitable for simple images with significant geometric features.

According to the above analyses, feature-based image matching obtains robust but sparse matching results, while area-based matching can obtain dense matching results but the matching reliability may depend on the texture conditions of the images. Therefore, this paper presents a hierarchical image matching method that combines the advantage of both the feature-based matching and the area-based matching methods and produces reliable and dense matching results with high efficiency and automation.

After the matching primitives are selected, the next task is to measure the similarity of the corresponding points in the image pairs, simulating human eyes by means of similarity measurement. The similarity measurement will be the matching score to judge the corresponding points or will be used for a global strategy to judge the corresponding points. There have been many similarity measurement for image matching presented in the past decades, such as the normalized cross-correlation (NCC) (Helava, 1978), sum of squares difference, normalised mutual information (Knops et al., 2006). These are simple computationally, but not distinct enough, and are sensitive to geometrical distortion and discontinuity problems. When using normalized cross-correlation to measure the similarity between the features on stereo images, an important problem is the selection of an appropriate window size to calculate the correlation values. So in this paper, NCC is selected as the matching score to measure the similarity between corresponding points of a stereo pair and the selection of window size will be discussed in experimental section.

III. DATA AND INSTRUMENTS

A. GPS DATA

These data were acquired in the field using a combination of standard surveying techniques (electronic distance measurement and GPS). The velocity vectors are overlaid on a subscene from the USGS 1 km AVHRR mosaic.

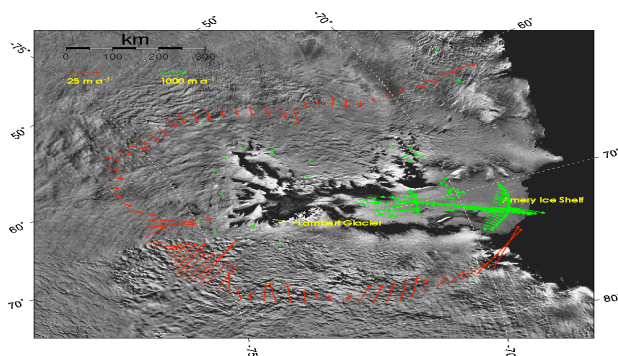


Figure 1-2

B. ICE VELOCITY THROUGH INSAR METHOD

Using RADARSAT SAR imagery obtained during the 2000 Antarctic Mapping Mission, ice velocity vectors were obtained over the Lambert Glacier. The areas of no motion (yellow) are either exposed land or stationary ice. The smaller confluent glaciers have generally low velocities (green, 100-300 meters per year) which gradually increase as they flow down the rapidly changing continental slope into the upper reaches of the faster flowing Lambert Glacier (click on ant-flyover-animation). Most of the Lambert itself has velocities between 400-800 meters per year, with a slight slowing in the middle section. As the glacier extends across the Amery Ice Shelf, velocities increase up to 1000-1200 meters per year as the ice sheet spreads out and thins. Only a handful of in situ velocity measurements have been previously reported of this huge glacier system. While the in situ and radar-derived measurements appear to be qualitatively similar, the extent and accuracy of the new measurements are unprecedented and provide quantitative baselines for future comparisons. The ice velocities are obtained from pairs of images obtained 24 days apart, using a technique called radar interferometry. This technique enables a highly precise alignment of image pairs that provides accurate measurements of topography as well as surfaces that have changed or moved over the short time interval, including glaciers.

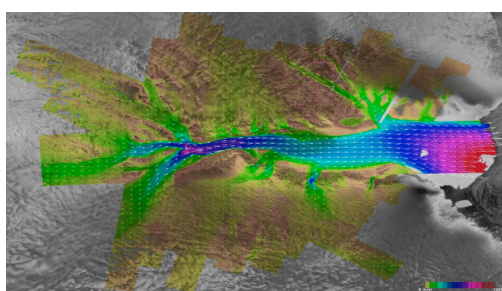


Figure 1-3

This data set, part of the NASA Making Earth System Data Records for Use in Research Environments (MEaSUREs) program, provides the first comprehensive, high-resolution, digital mosaic of ice motion in Antarctica assembled from multiple satellite interferometric synthetic-aperture radar data. Data were acquired during the International Polar Year 2007 to 2009.

This map was built from spring 2009 data from the Canadian Space Agency (CSA)'s and MacDonald,

Dettwiler and Associates Ltd. (MDA)'s RADARSAT-2, spring 2007-2008-2009 data from European Space Agency (ESA)'s Envisat Advanced Synthetic Aperture Radar (ASAR), and fall 2007-2008 data from the Japan Aerospace Exploration Agency (JAXA)'s Advanced Land Observing Satellite (ALOS) Phased Array type L-band Synthetic Aperture Radar (PALSAR), complemented by patches of CSA's RADARSAT-1 data from fall 2000 and ESA's Earth Remote Sensing Satellites ERS-1 and -2 data from spring 1996. Each radar instrument contributes its unique coverage and performance level. The final mosaic assembles 900 satellite tracks and more than 3,000 orbits of radar data. Data acquisitions between 2006 and 2011 are courtesy of the IPY Space Task Group.

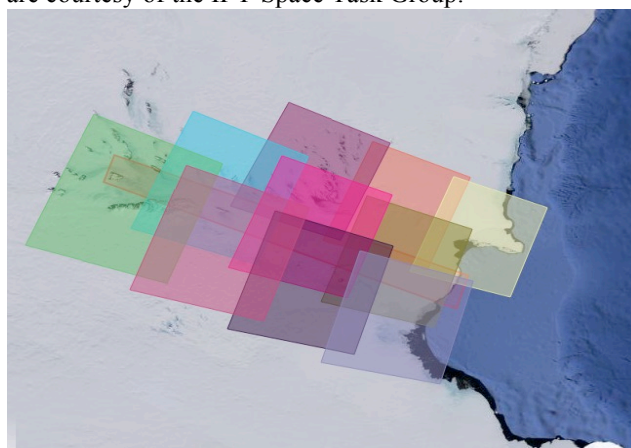


Figure 1-4

C. LANDSAT IMAGERY

Table 1: The Landsat7 images used in the analysis

GPS data (Table 2) used for validation were acquired in 1991[8] and 1997-2000 (unpublished) as part of various campaigns conducted over the AIS (see Figure 1-2 for locations).

IV. MATCHING SCHEME

A. Overview of the approach

The inputs for this approach are the images and rational polynomial coefficient (RPC) parameters. The

pat h	row	image 1	Image 2
128	112	L7212811220 011114	L72128112200 21219
128	109	LE712810920 02321SGS00	LE7128109200 1334SGS00
128	110	LE712811019 99361SGS00	LE7128110200 1334SGS00
128	111	LE712811119 99361SGS00	LE7128111200 2321SGS00
127	109	LE712710920 12038PFS00	LE7127109201 3056PFS00

workflow as shown in Fig. 1 includes the following steps:

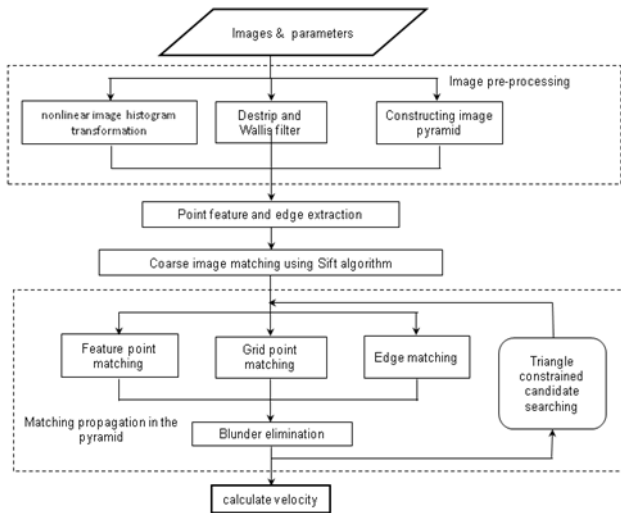


Figure 4-1. Workflow of our image matching procedure

(1) Image pre-processing including image transformation from 16-bit to 8-bit, the Wallis filter and constructing image pyramid.

(2) Feature point extraction using the Förstner. This step is performed to provide the interest points and edges for later image matching.

(3) Coarse image matching using Sift algorithm. This step is employed to generate the initial triangulation for image matching.

(4) Matching propagation in the image pyramid. This step includes feature point and grid point matching.

(5) Blunders elimination in each level including local smooth constraint of parallax and bidirectional image matching.

(6) Least squares image matching in original image level. By means of correcting radiometric and geometric distortion for images, not only is the matching precision improved but also enhance robustness by the rejection of blunder.

This paper will carry on the analysis from the following several important aspects about the approach.

B. Image pre-processing

The quality of matching results relies heavily on the quality of the images. Poor contrast would reduce the number of interest points extracted. The Wallis filter is employed to strongly enhance and sharpen the already existing texture patterns and increase the signal-to-noise ratio, which is beneficial for feature extraction.

At present, the grey values of panchromatic remote sensing images are stored by 16-bit. However, in our research, 8-bit stored images are necessary for the computation of image matching and the display of images in order to decrease calculation amount. So the 16-bit images are mapped to 8-bit images using a principle of auto levels.

After that, we must construct the image pyramid before matching. There are two kinds of methods for generating image pyramid: the direct method and the filtering method. The direct method is to transform 2

pixels by 2 pixels to 1 pixel with an average value. Filtering method, which is adopted in this paper, varies from the first one in that low-pass filtering is used to replace the average. Specifically, starting with the original image, each subsequent level of the image pyramid is created by sub-sampling the previous level image and smoothed by a Gaussian filter. Lower level images have coarser resolution and details are lost due to smoothing. The pyramid level number is a pre-defined value which could be either a user-input or can be determined according to the height range of the imaging area.

C. hierarchical image matching

The hierarchical searching algorithm is by narrowing the search scope to achieve the purpose of reducing the computational complexity to improve matching speed. It is proposed just as people find things with the coarse-to-fine strategy.

The hierarchical image matching method firstly uses a SIFT algorithm and RANSAC approach to obtain a few reliable correspondences, and then construct an initial triangulation. The SIFT algorithm (Lowe, 1999) is proved to be able to produce robust but relative sparse corresponding points invariant to moderate scale changes or distortions, which is ideal for the purpose of generating a certain number of well distributed matching points for the initial triangulation. In the SIFT descriptor, each interest point is characterized by a vector with 128 unsigned eight-bit numbers generated from a local region, which defines the multi-scale gradient orientation histogram. The matching is performed by measuring the similarity between the two vectors associated with the two matching points.

The RANSAC approach is used to detect and eliminate possible blunders from the previous SIFT matching results. It starts by randomly selecting a subset of the matched corresponding points. From the chosen matched points, a fundamental matrix can be calculated based on which a model is then built. This model is evaluated by determining whether each pair of corresponding points fit reasonably well to it. This is used as a criterion to determine the best model which has the largest number of correct corresponding points. This process is repeated to find the best model. Those matched points which do not fit for the final best model are considered as blunders and eliminated from the initial matching point set (Wu, et al., 2012).

After the seed points are extracted at the top level, an initial triangulation can be constructed and an area-based image matching with feature points and grid points is conducted at the top level again.

In the process of hierarchical strategy, image matching is first conducted on the lowest resolution. The matched points are then transferred to the next level (of higher resolution) where additional feature points could be matched. This process repeats until it reaches up to the original image level. At a subsequent level, points from upper level are matched again to achieve higher precision. A TIN (Triangulated Irregular Network) surface of parallaxes is generated from these matched

points using the Delaunay triangulation. This TIN is used to estimate the correspondence of additional feature points (Hwangbo J. W., 2010).

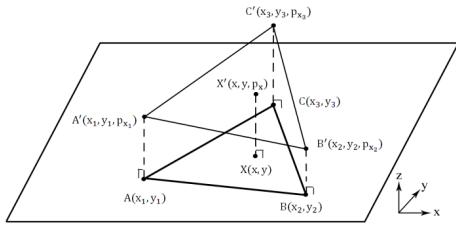


Figure 4-2. Interpolation of x parallax using TIN surface

As shown in Fig. 4, a point $X(x, y)$ is inside of a Delaunay triangle formed by points $A(x_1, y_1)$, $B(x_2, y_2)$, $C(x_3, y_3)$, the x parallax is interpolated based on the TIN surface formed by $A'(x_1, y_1, p_{x1})$, $B'(x_2, y_2, p_{x2})$, $C'(x_3, y_3, p_{x3})$. The x parallax of point $X(p_x)$ is interpolated as the z coordinate of point X' , which is the intersection between the 3-D plane $A'B'C'$ and the line XX' parallel to z axis. Parallax in y direction (p_y) can be calculated using the same strategy, only using y parallax as z coordinates. Finally, the estimated corresponding point coordinate (x', y') is defined as:

$$\begin{aligned} x' &= x + p_x \\ y' &= y + p_y \end{aligned} \quad (1)$$

D. Feature point and grid point matching

Förstner operator is one of the most famous operators to extract feature point and it has high speed and positioning accuracy. Förstner operator generates a series of feature points by identifying distinctive variations of pixel brightness values. The detected feature points including corners and round dots can reflect the shape of the terrain in the images. Feature points are typically found around shadow, where significant change of brightness values occurs. These points are related to the shape of terrain or objects such as ridges and rocks.

Feature point matching is very efficient and suitable in texture-rich regions with grey value variation. On the other hand, in image regions with poor texture or no texture information, few or even no feature points can be extracted. Thus, feature point matching will lead to holes in these areas. To solve this problem, grid points can be used and grid point matching has been introduced.

Grid points are points determined at given positions that are generally uniformly distributed over the whole image. Compared to the feature points, the choice of grid points is blind and thus many grid points may lie in poorly textured regions or occluded areas. The search for the match of a given grid point has a higher possibility of yielding an ambiguous match and even no matching

candidates. The grid points are also matched using cross-correlation following the coarse-to-fine strategy.

E. Blunder elimination

Even though the constraint of epipolar line and triangle is adopted in the process of image matching, still it cannot guarantee all the matching results are right. So it is important to employ an algorithm for detecting and removing outliers.

At first, bidirectional image matching algorithm is imbedded in our program. The basic idea of this strategy is simple as follows: First, a point in left image is taken as target point and find out the point of maximum similarity in right image. Then take the matched point (the point in right image) as target point and search for the best point in left image in the same way. Finally, we accept it if the two results overlap, or give it up as mismatch.

Although bidirectional image matching method eliminates some wrong matches, there still exist some mismatched points. Therefore, local smooth constraint of parallax is adopted in this research. The logic behind the strategy is that the terrain is continuous and spatially correlated in a small area. Speaking specifically, for every pair of corresponding image point, the adjacent corresponding points within a certain distance are used to fit an optimal plane of parallax. Outliers are the values that are statistically far from most others in a set of data. Since the spatial distribution pattern of the parallax of corresponding points could vary depending on the type of local terrain, the parallax offset from the fitted plane is compared with the standard deviation of the neighboring points. If the offset is beyond 3σ , the matched point is considered as a blunder and discarded from the result.

V. EXPERIMENT RESULT

We have applied the proposed matching approach to Landsat stereo images for ice surface motion measurement in AIS, East Antarctica. The resolution of the images is 15 m. The scene covers a total area of 175km by 350 km and consists of a variety of land cover types, including blue ice, ice-free rock, crevasse, snow and firns, water body and moraine.

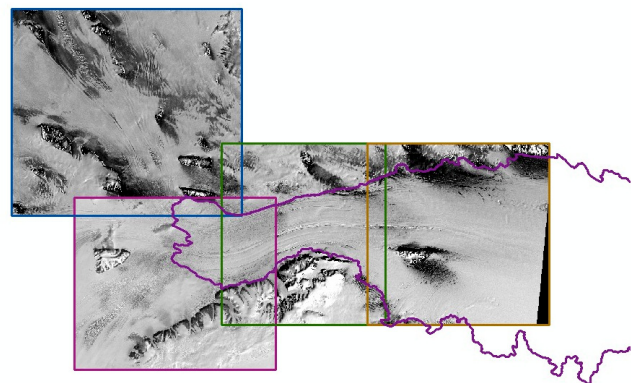


Figure 5-1. Landsat7 image of AIS, Antarctica

Controlling the matching parameter setting is important for high quality matching generation. Since the stereo matching result is highly dependent on the properties of input data, there is no single set of parameters that is perfect for every image (Hwangbo J. W., 2010). So Table 1 shows some comparatively optimal parameters we selected through many experiments.

Level	1	2	3	4
Image scale	1/8	1/4	1/2	1
Matching window size	11×11	13×13	15×15	15×15
Search window size	11×11	9×9	7×7	7×7
Correlation coefficient threshold	0.8	0.8	0.8	0.7

Table 1. Selected parameters for hierarchical image matching



Figure 5-2. Matched points in hierarchical image pyramid

Fig. 5-2 shows the matched points including feature points and grid points at each hierarchical matching level. They provide robust structure of terrain from coarse level

Station	Lat(S)	Lon(E)	GPS	MEaSURE	HMV
TS06 (2000/01)	73.40	66.68	496	362	477
TS05 (2000/01)	73.25	67.07	768	757	745
v5 (1997/98)	72.98	67.48	715	681	657
v3 (1997/98)	72.61	67.57	623	667	609
GA29 (1991)	71.92	68.67	382	408	365
GA35 (1991)	71.84	68.43	395	399	376

with a few points to finer level with an increased amount of detail. Fig. 5-3 illustrates the generated HMV(Hierarchical Matching Velocity) with Rignot published velocity field. Because many areas have cloud cover or significant changes, there are many blunders in these areas. Figure 5-4 illustrated the velocity field. This velocity field is generated from the matched points using triangular linear interpolation approach. Visual inspection reveals that good results have been achieved.

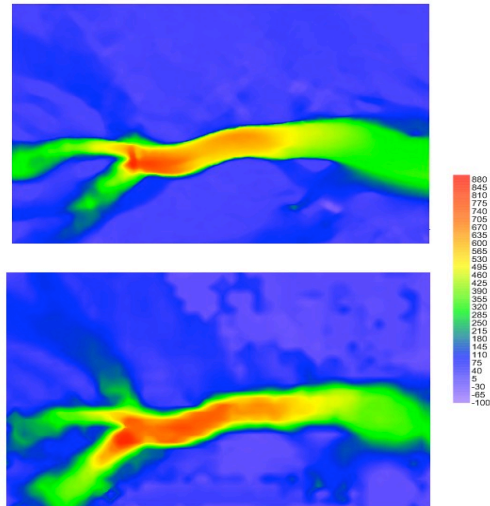


Figure 5-3. A comparison of our result(below) with Rignot published(above)

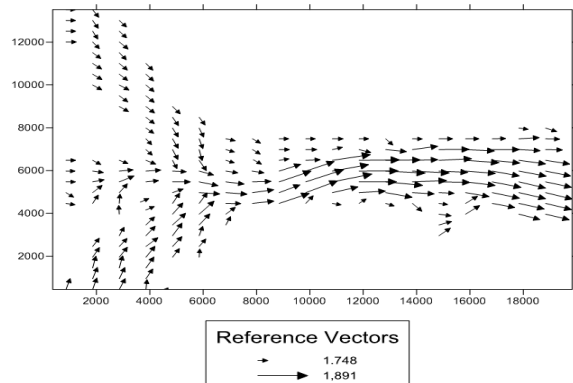


Figure 5-4. ice velocity field illustrated in vector form
 Finally, six position both have GPS, MEaSURE and HMV(Hierarchical Matching Velocity) value was selected and checked to ensure that these automatically matched velocity. In this area, points were manually matched in the stereo images for generating a manual matching velocity. Then GPS, MEaSURE and manual matching velocity was compared with the HMV generated from automatically matched points in the of profile.. Overall, the velocity result from 4 different methods showed high consistence. The differences between manually and automatically generated velocity field were in the range of ± 25 maximum with standard deviation less than 6m. The random elevation errors of such magnitude are reasonable, considering that the pixel resolution of the raw images is about 15m.

Table 2: Comparison of Velocities (m/year) for GPS/MEaSURE/HMV(Hierarchical Matching Velocity)

VI. AIS ICE FLUX CALCULATION

By calculating the Lambert Glacier Basin, ground line output flux material, shall calculate the ground line Amery Ice Shelf ice flux. For floating ice shelf, the surface velocity and ice under the surface along the

vertical direction of the velocity and flow of various points can be approximated as identical, and secondly, the flow rate of each point are essentially the same, are similar to the cross-sectional direction; once again, at the bottom did not like the undulating ground ice, which can be considered as approximate plane. Based on the above conditions, we can establish the model shown in Figure 6-1. Therefore, the calculation section ice flux is actually calculated by the cylinder as shown in irregular quality of the ice contained, if the ice flow and cross flow direction is not perpendicular to the section, the flux result need to multiply $\sin\theta$. Section i of the ice flux is calculated as

$$Flux_k = Thick_k \cdot Density_k \cdot Width_k \cdot Velocity_k \sin \alpha_k$$

In the formula, θ is the angle of the ice flow direction between the section.

Ice at the bottom of the ice surface velocity of flow is 0.8 times, and the ice surface to the bed of ice flow on the vertical variation of uniform size, equivalent to the entire surface of the cylinder, the average velocity of the flow rate of 0.9 times.

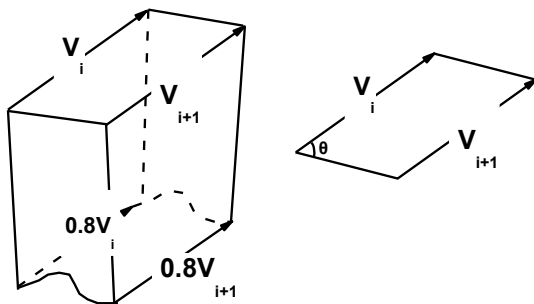


Figure 6-1

Therefore, the calculation of the Lambert Glacier Basin, ground line output flux material requirements for the major InSAR ice velocity data, the ice thickness data, ice density data. Ice thickness data is the use of hydrostatic fluid balance formula, derived from the Amery Ice Shelf DEM obtained. Because the data distribution and spatial interpolation error is generated when the DEM, geoid model OSU91a (error of about 3m) and ice density data uncertainties (error of about 5kgm⁻³), calculated by the DEM in some parts of the ice thickness 100 ~ 200 m possible errors. The flow rates of data error of about 5-10 m a⁻¹. Taking all the above errors ice flux across the grounding line total error is set to 10% (Wen et al., 2007). It can be concluded that the entire Lambert Glacier Basin, ground line ice flux of about 88.9 ± 8.9 Gt/a.

VII. DISCUSSION AND CONCLUSIONS

This paper presented a triangulation based hierarchical image matching method for stereo satellite imagery. Table 2 gives the accuracy evaluation results in the whole rectangular region mentioned above. About

94% of the region is within three standard deviations though the maximum absolute difference is 4.841m.

Though the experiment using Landsat7 ETM images, we draw the following conclusions:

(1) The SIFT algorithm with RANSAC approach can produce reliable but sparse corresponding points which is ideal for obtaining the initial values for hierarchical image matching.

(2) The hierarchical matching strategy based on triangulation constraint proved to be effective and reliable especially in some area with poor and repetitive texture. More importantly, for stereo satellite imagery, the hierarchical search strategy can improve the speed of image matching; otherwise it will be very time consuming to search corresponding points in the original image.

(3) The experiment results showed that local smooth constraint of parallax can eliminate most of outliers effectively, although there still exist some mismatches. Future work will be focused on this problem to better refine the matching results.

The widespread retreat of glaciers can be considered as a response to the climate change. Being the largest retreating glacier-ice shelf system in East Antarctica, the Amery Ice Shelf-Lambert Glacier system plays an important role in contributing to sea level rise as well as the surrounding environment and climate. The present study is focused on the investigation of the stability of Amery ice shelf and Lambert glacier system, mainly surface ice flow field flux calculated. Global warming leading to increased Antarctic glacier change, flow speed up, greater flux. Article does not consider the surface melting and freezing, because studies show that the main mass lose through under ice melt and glaciers flow. Future, if considering the cumulative rates of sedimentation can get estimates of the mass balance .

ACKNOWLEDGMENT

I would like to gratefully acknowledge the enthusiastic supervision of Dr Ron Li during this work. I thank Prof Weian Wang for the technical discussions. This document's development has been supported by the polar 973 project, and peer reviewed by Associate Professor Qiao.

REFERENCES

- [1] Budd, W.F. and Corry, M.J. and Jacka, T.H. Results from the Amery Ice Shelf Project. *Annals of Glaciology* 3 (1982), 36-41
- [2] Kiernan, Rob Ice Sheet Surface Velocities Along the Lambert Glacier Basin Traverse Route. Antarctic Cooperative Research Centre and Australian Antarctic Division, Research Report No. 23, May 2001.
- [3] Fricker, Helen A. and Warner, Roland C. and Allison, Ian Mass budget of the Lambert Glacier-Amery Ice Shelf system, East Antarctica: a Comparison of Computed Balance Fluxes and Measured Fluxes. *Journal of Glaciology* 46,155 (2000), 561-570. <http://dx.doi.org/10.3189/172756500781832765>
- [4] Manson, R. and Coleman, R. and Morgan, P.J. and King, M.A. Ice Velocities of the Lambert Glacier from Static GPS Observations. *Earth, Planets and Space* 52,11 (2000), 1031-1036.
- [5] Scambos T, Hulbe C, Fahnestock M and Bohlander J 2000 The link between climate warming and break-up of ice shelves in the Antarctic Peninsula : *J. Glaciology*. 46 510-530. <http://dx.doi.org/10.3189/172756500781833043>

- [6] Young, N.W. and G. Hyland. 2002. Velocity and strain rates derived from InSAR analysis over the Lambert Glacier - Amery Ice Shelf system. *Annals of Glaciology*, 34, 228-234. <http://dx.doi.org/10.3189/172756402781817842>
- [7] Hwangbo J. W., 2010. Integration of Orbital and Ground Imagery for Automation of Rover Localization. *PhD Dissertation*, The Ohio State University, pp. 115-152.
- [8] Jiang, W., Zhang, J., Zhang, Z., 2008. Simulation of three-line CCD satellite images from given orthoimage and DEM. *Geomatics and Information Science of Wuhan University*, 33(9), pp. 943-946.
- [9] Lowe, D G., 2004. Distinctive image features from scale-invariant keypoints. *International Journal of Computer Vision*, 60(2), pp. 91-110. <http://dx.doi.org/10.1023/B:VISI.0000029664.99615.94>
- [10] Poon, J., Fraser, C., Zhang, C., Zhang, L., Gruen, A., 2005. Quality Assessment of a Digital Surface Model Over Urban Areas Generated from IKONOS Stereo Pair. *The Photogrammetric Record*, 20(110): 162-171. <http://dx.doi.org/10.1111/j.1477-9730.2005.00312.x>
- [11] Tang, L., Wu, C., Chen, Z., 2002. Image dense matching based on region growth with adaptive window. *Pattern Recognition Letters*, 23, pp. 1169-1178. [http://dx.doi.org/10.1016/S0167-8655\(02\)00063-6](http://dx.doi.org/10.1016/S0167-8655(02)00063-6)
- [12] Wu, B., Zhang, Y., Zhu, Q., 2012. Integrated point and edge matching on poor textural images constrained by self-adaptive triangulations. *ISPRS Journal of Photogrammetry and Remote Sensing*, 68, pp. 40-55. <http://dx.doi.org/10.1016/j.isprsjprs.2011.12.005>
- [13] Wu, B., Zhang, Y., Zhu, Q., 2011. A Triangulation-based Hierarchical Image Matching Method for Wide-Baseline Images. *Photogrammetric Engineering & Remote Sensing*, 77(7), pp. 695-708.
- [14] Zhang, L., Armin G., 2006. Multi-image matching for DSM generation from IKONOS imagery. *ISPRS Journal of Photogrammetry & Remote Sensing*, 60 ,pp. 195-211. <http://dx.doi.org/10.1016/j.isprsjprs.2006.01.001>
- [15] Zhang, L., Gruen, A., 2004. Automatic DSM generation from linear array imagery data. *The International Archives of the Photogrammetry, Remote Sensing and Spatial Information Sciences*, Beijing, China, Vol. XXXV. Part B3, pp. 128-133.
- [16] Zhang, C., Fraser, C., 2008. Generation of digital surface model from high resolution satellite imagery. *The International Archives of the Photogrammetry, Remote Sensing and Spatial Information Sciences*, Beijing, China, Vol. XXXVII. Part B1, pp. 785-790.
- [17] Zhang, C., Baltsavias, E., 2000. Knowledge-based image analysis for 3D edge extraction and road reconstruction. *International Archives of Photogrammetry and Remote Sensing*, Amsterdam, Netherlands, Vol. XXXIII, Part B3/2, pp. 008-101.
- [18] Zhang, C., Fraser, C., 2009. An improved approach for DSM generation from high resolution satellite imagery. *Journal of Spatial Science*, 54(2), pp. 1-13. <http://dx.doi.org/10.1080/14498596.2009.9635175>
- [19] Zhang, Z., Zhou, Y., 1989. Epipolar line of SPOT images using fitting method. *Journal of Wuhan University of Surveying and Mapping Technology*, 14(2), pp. 20-24.

AUTHORS

Yi Liu is with Tongji University, Shanghai, China (e-mail: 07liuyi@tongji.edu.cn). He is a PhD candidate at College of Surveying and Geo-Informatics, Tongji University. He received his Bachelor's Degree in Computer Engineering, and his Master's Degree in Mechatronics Engineering from Huazhong University of Science and Technology.

Fei Yan is with Tongji University, Shanghai, China (e-mail: 2011feiyan@tongji.edu.cn). He is Second year graduate students in College of Surveying and Geo-Informatics, Tongji University. He received his undergraduate degrees in Surveying and mapping engineering from Tongji University.

This work was supported by National Key Basic Research Program of China (No. 2012CB957701) and The National High Technology Research and Development Program of China (No.2012AA12A305). Comments to the manuscript from the referees are greatly acknowledged. Submitted, 14 August, 2013. Published as resubmitted by the authors on 16 September 2013.